MODELING THE BEHAVIOR OF OPTICAL ELEMENTS IN RADIATION ENVIRONMENTS

Thomas A. Barlow
Clifford E. Rhoades, Jr.
Lawrence Livermore National Laboratory

UCRL--95946

DE87 005053

Milton Merker
John R. Triplett
S-Cubed, A Division of Maxwell Labs., Inc.

ABSTRACT

Calculation of heating caused by the deposition of X-rays in thin film optical elements is complicated because the mean free path of photo and autoionization electrons is comparable to the thin film thickness and thus the electron deposition cannot be considered local. This paper describes the modeling in a 1-D code of a) X-ray deposition and transport, b) electron production, deposition and transport, and c) thermal conduction and transport. X-ray transport is handled by multigroup discrete ordinates, electron transport is done by the method of characteristics, applied to the two term spherical harmonics expansion approximation (P1) to the Spencer-Lewis transport equation, and thermal transport is computed by a simple Richardson extrapolation of a backward Euler solution to the heat conduction equation. Results of a few test cases are presented.

I. INTRODUCTION

Space based strategic defense systems are expected to require the fielding and survival of optics in adverse natural as well as hostile environments. A coordinated experimental and theoretical effort is underway at Livermore under the leadership of G. Richard Wirtenson to characterize optical surfaces[1] and to understand the behavior[2] of optical elements exposed to X-rays. In this paper, part of our theoretical program to calculate the effects of X-rays on optics is presented. In this paper, we describe the XRT[3-5] (X-Ray Transport) computer code for modeling the behavior of optical elements in radiation environments. Developed at S-Cubed in LaJolla by John R. Triplett, XRT uses deterministic methods to calculate energy dose, and temperature response given a one dimensional material configuration and an incident X-ray flux. Results of a few test cases of model optics designs exposed to several model spectra X-ray fluences are presented. Comparisons with the GENRAT-DEAP[6-8] and TFT[9-11] codes are included. X-ray deposition results are also compared with those calculated by TART.[12,13] Section II provides an overview of the XRT physics and numerical methods. In Sec. III the X-ray deposition process is outlined. Section IV describes the production of electrons. Section V discusses the transport of electrons. Section VI contains the discussion of thermal conduction. Section VII outlines the model problems, while Sec. VIII contains an overview of the data and parameters. Section IX describes the results, and Sec. X gives the conclusions.

II. XRT PHYSICS AND METHODS

The calculation of heating caused by the deposition of X-rays and the resulting thermal behavior represents a somewhat more complicated exercise than typical of most standard modeling efforts. The reason for this is straightforward. The mean free path of photo and autoionization electrons is comparable to the thickness of the thin films and thus the deposition of electrons cannot be considered local. Both the electron and heat transfer processes convey large amounts of energy for short distances, and are essential to the analysis when the spatial scale of interest is sufficiently small, as it is in the case of optical coatings.

The XRT physics and methods are summarized in Table I.

TABLE I. XRT physics and methods.

Physics	Method
X-ray Deposition	Multigroup discrete ordinates
Electron Production	Simplified probability model
Electron Transport	Method of characteristics applied to two term spherical harmonics expansion to Spencer-Lewis equation
Thermal Conduction	Richardson extrapolation of backward Euler solution of heat conduction equation

Specifically, XRT models in one spatial dimension the physics of X-ray deposition, electron transport, and thermal conduction. It handles X-ray deposition by the multigroup discrete ordinates method. It does electron transport by the method of characteristics, applied to a two-term spherical harmonics expansion approximation (P1) of the Spencer-Lewis electron transport equation. Thermal transport is obtained by a simple Richardson extrapolation of a fully implicit backward Euler solution of the heat conduction equation.

III. X-RAY DEPOSITION

The X-ray deposition phase of XRT uses the method of discrete ordinates to solve the transport equation in one spatial dimension. The fluence in angle interval i and energy group j is given by

$$\phi_{ij}(x) = \int_0^\infty dt \int_0^{2\pi} d\phi \int_{\mu_i}^{\mu_{i+1}} d\mu \int_{E_j}^{E_{j+1}} \mu I(x,E,\Omega,t)\, dE$$

where I is the energy intensity distribution, μ is the normal direction cosine, ϕ is azimuth, t is time, and E is photon energy. The incident beam is depleted by Compton scattering and photoelectric absorption. Coherent scattering and inverse bremsstrahlung are not included. As the beam passes through the material, the scattered flux emitted into each angle-energy interval is determined. Fluorescent photons are emitted and the process is repeated for secondary photons.

IV. ELECTRON PRODUCTION

Since Compton absorption is an important process only for photon energies above the range of primary interest, Compton contributions are included as a local dose only.

The number of photoionizations Q, per gram of material per incident fluence is given by

$$Q = \sum_{i,j} \left[\frac{\phi_{ij}}{E_j \mu_i}\right] \cdot [\text{mass fraction}] \cdot \sigma_{PE}$$

where ϕ_{ij} is the fluence in angle interval i and energy group j, E_j is the photon energy, μ_i is the direction cosine and σ_{PE} is the photoelectric cross section per unit mass of the element.

Given Q photoionizations per gram of material due to absorption of photons with mean energy hv in a particular elemental component, there results $P_k Q$ photoelectrons of energy $hv-V_k$ where V_k is the binding energy of subshell k and P_k is the fractional photoelectric yield of the k subshell.

Obviously P_k vanishes for hv less than V_k. XRT assumes that P_k is constant for hv in the range $V_k \le hv < V_{k-1}$ and independent of vacancies already present in the atom.

XRT uses tables of decay rates for fluorescent transitions from the K and L shells and autoionization from the K, L, and M shells. Autoionization dominates in low Z elements, while fluorescence dominates in high Z elements. In autoionization, an initial electron vacancy causes a transition of a higher electron and ejection of another. There are two types of autoionization: Coster-Kronig, where at least one electron comes from the same main shell as the initial vacancy, and Auger, otherwise. XRT uses 19 subshells, K, L1-3, M1-5, N1-5, N6N7, O1-3, O4O5.

V. ELECTRON TRANSPORT

In one dimension, the Spencer-Lewis transport equation for electrons is:

$$\frac{\partial f}{\partial s} + \mu \frac{\partial f}{\partial x} = \int d\Omega' \, \sigma(x,s,\Omega' \cdot \Omega)\,[f'-f] + q(x,s,\Omega)$$

where s is the path length of electrons with energy (E) given by $r_o - r(E)$, r is the residual range of electrons with energy (E), μ is the normal direction cosine, Ω is the direction unit vector, x is the spatial coodinate, σ is the cross section for single scattering, q is the electron source, and f is the distribution function, that is, the number of electrons at depth x per unit transverse area, per unit residual range, per unit solid angle. Here, f is $f(x,r,\Omega)$ and f' is $f(x,r,\Omega')$.

Integrating the Spencer–Lewis equation with respect to electron direction Ω, once as it stands and once again after multiplying through by μ, and using the P_1 approximation in which f and q are represented by the first two terms of their expansions in spherical harmonics, namely

$$f(\Omega) = \frac{1}{4\pi}(f_0 + 3\mu f_1)$$

$$q(\Omega) = \frac{1}{4\pi}(q_0 + 3\mu q_1)$$

we obtain the following reduced system of equations for the Spencer–Lewis equation

$$\frac{\partial f_0}{\partial s} + \frac{\partial f_1}{\partial x} = q_0$$

$$\frac{\partial f_1}{\partial s} + \frac{1}{3}\frac{\partial f_0}{\partial x} + \sigma_t f_1 = q_1$$

where

$$f_0 = \int f d\Omega \qquad f_1 = \int f \mu d\Omega$$

$$q_0 = \int q d\Omega \qquad q_1 = \int q \mu d\Omega$$

and

$$\sigma_t = \int \sigma d\Omega - \int \sigma \mu d\Omega.$$

The reduced system now comprising the Spencer–Lewis equation is then solved by the method of characteristics, where we have made the approximation that q_1 is zero. This is a reasonable approximation since the first angular moment of the source, q_1, is strictly zero for electrons produced by autoionization and is small for photoelectrons except at high energies. The required boundary conditions are that the spectral fluence ϕ and current J are continuous at material interfaces where

$$\Phi(E) = f_0(s)/|dE/ds|$$

$$J(E) = f_1(s)/|dE/ds|$$

VI. THERMAL CONDUCTION

In one dimension, the thermal conduction equation is

$$-\rho C \frac{\partial T}{\partial t} + \frac{\partial}{\partial x}\kappa \frac{\partial T}{\partial x} + \rho D_0 \frac{\partial \Phi}{\partial E} = 0$$

where T is temperature, ρ is density, ρC is specific heat per unit volume, κ is heat conduction coefficient, D_0 is absolute dose, and $\Phi(t)$ is fraction of total dose deposited before time t. The thermal conductive equation is solved at each point x_i at time t_{n+1} using the backward Euler method which is unconditionally stable and first–order accurate. Richardson extrapolation is used to give a second order answer. Specifically,

$$F^{(3)} = 2F^{(2)} - F^{(1)}$$

where $F^{(1)}$ is the result of a single backward Euler step, $F^{(2)}$ is the result of two successive backward Euler half–steps, and $F^{(3)}$ is the second order accurate answer.

VII. THE MODEL PROBLEMS

Two different types of model problems are employed in the calculations described in this paper. One type has a fused silica substrate of .5 cm with a beryllium energy sharing layer of 1000 nm and a reflective overcoating, either aluminum or gold, of 75 nm and 125 nm, respectively. The other consists of a heavy metal, either gold or molybdenum, substrate of .5 cm with an aluminum layer of 75 nm and an overcoating of aluminum oxide of 150 nm. There are, thus, a total of four model optical element designs. These are depicted in cross section in Fig. 1.

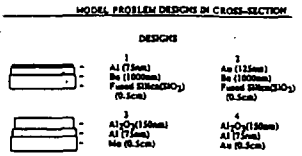

FIGURE 1.

In addition to the model optical element designs, it is necessary to specify model spectra, fluence, pulse shape and duration. There are three basic types of model spectra – argon, monoenergetic and blackbody. The argon spectrum is a model of the output of the Blackjack V simulator at Maxwell Laboratories in San Diego. Its pulse has an isosceles triangular shape with a base of 28.6 ns. Two fluences, .1, and .5 cal/cm^2, are employed in the calculations. For the monoenergetic spectra, no thermal calculations are intended. Hence, no fluence, pulse shape or duration are specified for them. Two blackbody spectra of 1 and 4 keV energy and .1 and .4 cal/cm^2 fluence, respectively, with a pulse duration of 10 ns are also used. For convenience, the model spectra are summarized in Table 2.

TABLE 2. Model problem spectra.

Type	Pulse Duration	Fluence (cal/cm²)	Reference Letter
Argon	28.6 ns	0.1 and 0.5	A
Monoenergetic (0.5, 1.0, 2.0, 5.0, 10.0, 20.0 and 50 keV)			B
1 and 4 keV Blackbody	10 ns	0.1 and 0.4 respectively	C

VIII. DATA AND PARAMETERS

Thermophysical data for the six materials used in the model problems are those of Childs.[14,15] The argon spectrum used in the calculation is that defined by Merker[16] in 37 specified energy bins with a normalized fraction of fluence in each energy bin and an isosceles triangular time pulse of 28.6 ns. The 1 and 4 keV blackbody integral spectra in 109 energy bins are also provided by Childs.[17]

The X-ray interaction data, provided by Watts,[18] are those of Biggs and Lighthill.[19] The Biggs and Lighthill X-ray interaction data are used in the GENRAT-DEAP, TFT, and XRT calculations. By contrast, TART calculations are based on the standard evaluated Livermore X-ray interaction data.[20]

The test set matrix of the calculations performed for the code comparison is shown in Table 3. The spectra are labeled by the letters A, B, and C across the top of Table 3. These letters identify the model spectra in Table 1 as given under the reference letter heading. The designs are labeled by the numbers 1, 2, 3, and 4 down the left hand side of Table 3. These numbers identify the model designs in Fig. 1. The presence of an "x" indicates that calculations are included in the test set. All cases have been run both with and without secondary effects, including fluorescence and electron production. Dose data have been compared for all cases. In addition, thermal and temperature data at the end of pulse have been calculated for the cases involving the argon and blackbody spectra.

IX. RESULTS

Representative computational results are displayed in Fig. 2 through Fig. 26. Figures 2 through 11 contain the results for the argon spectrum calculations. Figures 12 through 16 contain the results for the monoenergetic deposition calculations. Figures 17 through 26 contain the results for the blackbody spectra calculations.

TABLE 3. Test set matrix.

Design	Spectra A	B	C
1	X	X	X
2		X	X
3		X	X
4	X	X	X

All cases run with and without secondary effects.
All cases provide dose data.
A and C include temperature at end of pulse. No temperature data for B.

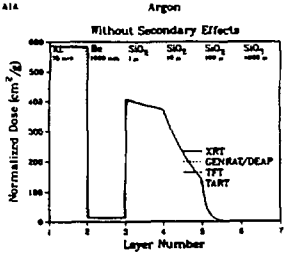

FIGURE 2.

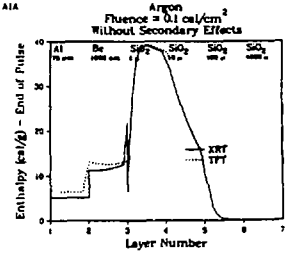

FIGURE 3

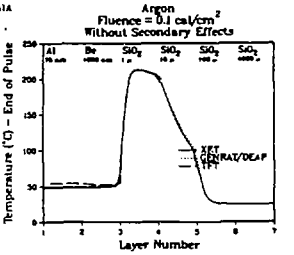

FIGURE 4

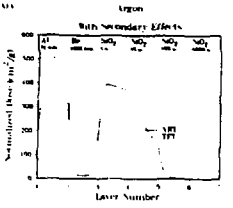

FIGURE 5

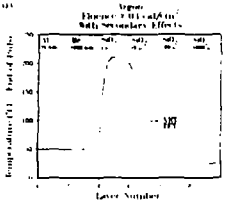

FIGURE 6

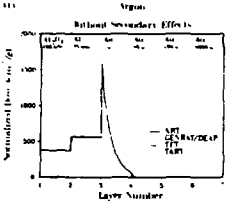

FIGURE 7

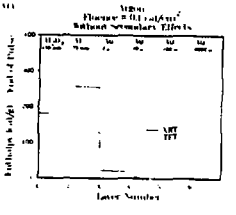

FIGURE 8

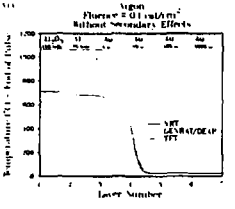

FIGURE 9

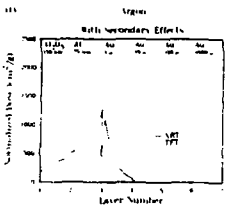

FIGURE 10

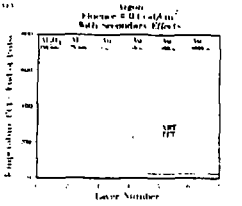

FIGURE 11

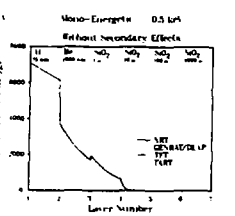

FIGURE 12

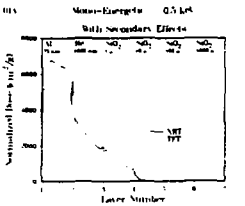

FIGURE 13

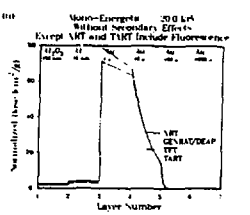

FIGURE 14

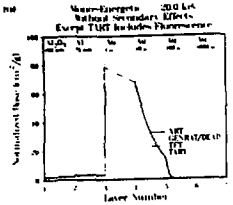

FIGURE 15

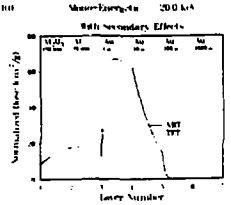

FIGURE 16

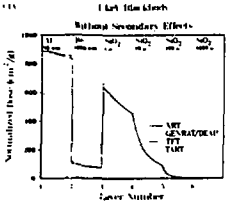

FIGURE 17

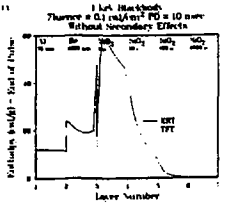

FIGURE 18

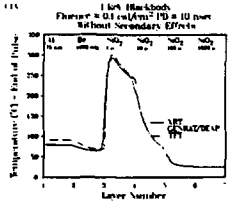

FIGURE 19

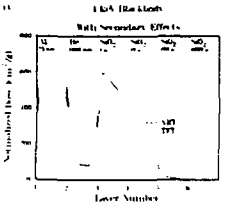

FIGURE 20

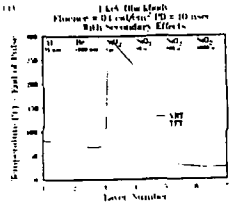

FIGURE 21

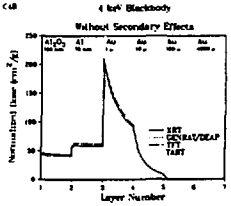

FIGURE 22

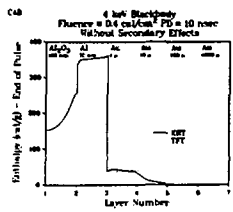

FIGURE 23

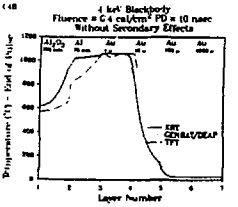

FIGURE 24

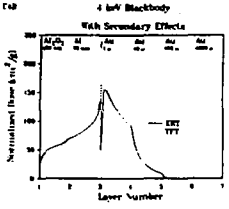

FIGURE 25

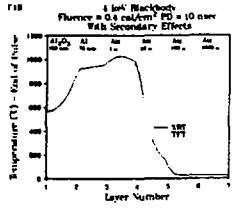

FIGURE 26

Figures 2 through 26 have the following format. One of these quantities, either normalized dose (cm^2/g), enthalpy (cal/g) or temperature (°C), is plotted versus layer number. Within each layer number the scale is linear. However, the scale changes from one layer number to the next. For example, in Fig. 2, layer number 1 consists of 75 nm of aluminum while layer number 2 consists of 1000 nm of beryllium. Thus, the distance between the numbers 1 and 2 on Fig. 2 is 75 nm, while the distance between the numbers 2 and 3 is 1000 nm. To aid the reader, the thicknesses and compositions of these layers are displayed at the top of each figure below the caption.

Results in Figs. 2 through 26 are displayed in the following systematic fashions. The first group of figures contains the calculations without secondary efforts. The second group of figures contains the calculations with secondary efforts. In temperature and enthalpy plots, the fluence level in cal/cm^2 is included in the caption. For monoenergetic and blackbody spectra, the energy is also included in the caption.

X. CONCLUSIONS

Based on the previously displayed results, we make the following observations. Once adequate spatial zoning is used and proper boundary conditions in the substrate are taken, the four computer codes are in extremely good agreement for the deposition part of the calculations. In the deposition calculations, the complicated nature of the blackbody, and argon spectra overwhelm any differences in methods or data. Consequently, the monoenergetic spectra model problems are vital to understanding computer code and data differences. For example, in runs where no secondary effects are to be included, we clearly see that fluorescence has been included in the XRT and TART calculations. This explains the differences between XRT and TART on the one hand and GENRAT/DEAP and TFT on the other, as displayed in Fig. 14, because fluorescence is an important effect in gold at 20 keV. It is also evident that the X-ray interaction data and use in the four codes are not identical. These cause a factor of 5 difference in dose, for example, in placement of the K-edge in molybdenum at 20 keV. Use as reflected in the interpolation scheme also causes a few percent difference. Although there are minor differences in X-ray dose calculations, none are large.

By contrast, there are large thermal and temperature differences which cannot be explained by the differences in dose. These differences are substantial in gold, while less so in molybdenum. There is reasonable agreement with fused silicon, however. We believe that these differences are largely caused by the methods used to treat the melting phenomenon in the various codes. Additional work is underway to verify these observations. The treatment of secondary electron production trans- port and deposition clearly differs between XRT and TFT. The differences are especially noticeable at the interface between a heavy metal such as gold and a light metal such as aluminum. Some preliminary calculations with the TIGERP electron photon Monte Carlo code which is expected to be valid only for energies above 1 keV are inconclusive. Results for 50 keV photon energy are similar to those of XRT whereas results at 20 keV lie half-way between those of TFT and XRT. We are currently investigating the sources of these differences.

For those concerned with designing survivable optics, we recommend the use of more than one code to calculate any specific design in a given environment. Additional work in tracking down the differences in secondary electron effects, for example, by inventing monoenergy electron dose problems, should be undertaken. Likewise, the thermal and temperature differences need to be fully understood.

XI. ACKNOWLEDGMENTS

This work was funded in part by the Strategic Defense Initiative Organization through the Air Force Weapons Laboratory and Rome Air Development Center and was performed under the auspices of the U. S. Department of Energy by the Lawrence Livermore National Laboratory under Contract W-7405-ENG-48. It is a great pleasure to acknowledge the contributions of Bill Childs at Aerospace, G. Richard Wirtenson, Ernest Plechaty, and Lila Chase of Lawrence Livermore National Laboratory, Boris Shkoller at S-Cubed, and Alan Watts. Carol Breen and Steve Sauer at Ktech to this work. At the Air Force Weapons Laboratory, our project officers are Maj Douglas Caldwell and Lt Richard Engstrom. At the Rome Air Development Center, Capt Michael Rau is our project officer. We are grateful to them for their support and encouragement during the course of this research.

REFERENCES

1. D. F. Edwards, C. H. Gillespie and G. R. Wirtenson, "Characterization of Optical Surface Degradation: The Angular Resolved Scatterometer (ARS)," Proc. of the High Power Laser Optical Components Conf. 29-31 October 1986, National Bureau of Standards, Boulder, CO.
2. G. R. Wirtenson, D. F. Edwards, and T. T. Saito, "Test Results for Nuclear Hardened Optical Coatings," Proc. of the High Power Laser Optical Components Conf. 29-31 October 1986, National Bureau of Standards, Boulder, CO.
3. J. R. Triplett, The XRT Code, S-Cubed, La Jolla, CA, SSS-R-83-5829 (1982).
4. J. R. Triplett, B. Shkoller, M. H. Rice, S. Shkoller, and M. Merker, XRTH, A Combination of XRT and Hydro Codes, S-Cubed, La Jolla, CA, SSS-R-86-7981 (1986).
5. J. R. Triplett, B. Shkoller, and M. Merker, XRTH Users Manual and Reference Guide, S-Cubed, La Jolla, CA, SSS-R-87-8420 (1986).
6. W. H. Childs, "GENRAT-DEAP," private communications, 1986.
7. E. H. Fletcher, Deposition of Radiation in Solids, Aerospace Corporation, Los Angeles, CA, ATM 68(3250-30)-1 (1967).
8. B. J. McFarland, Differential Equation Analyzer Program, Volume 1, Advanced Systems Department, 589, Rocketdyne, Los Angeles, CA, LAP-69-552(RC) (1969).
9. A. J. Watts, Thin Film Computer Code Development, The TFT Routine - Thin Film Transport: Part I - Background and Theory, Ktech Corporation, Albuquerque, NM, Ktech TR 83-19 (1984).
10. A. J. Watts, C. M. Breen, and S. K. Sauer, Thin Film Computer Code Development, The TFT Routine - Thin Film Transport: Part II - Thermal Conduction and Stress Response, Ktech Corporation, Albuquerque, NM, Ktech TR 86-04 (1986).
11. A. J Watts, C. M. Breen, and S. K. Sauer, Thin Film Computer Code Development, Part III - PUFF TFT - A Material Response Computer Code Users Manual and Subroutine Descriptions, Ktech Corporation, Albuquerque, NM, Ktech TR 85-16 (1986).
12. E. F. Plechaty and J. R. Kimlinger, TART-NP: A Coupled Neutron- Photon Monte Carlo Transport Code, Lawrence Livermore National Laboratory, Livermore, CA, UCRL-50400, Vol. 14 (1976).
13. J. R. Kimlinger and E. F. Plechaty, TART and ALICE Input Manual, Lawrence Livermore National Laboratory, Livermore, CA, UCID-17026, Rev. 2 (1986).
14. W. H. Childs, Thermophysical Properties of Selected Space-Related Materials, Aerospace Corporation, Los Angeles, CA, TOR-0086 (6435-02)-1 Vol. 1 (1981).
15. W. H. Childs, Thermophysical Properties of Selected Space-Related Materials, Aerospace Corporation, Los Angeles, CA, TOR-0086 (6435-02)-1 Vol. 2 (1986).
16. M. Merker, private communication, 4 June 1986.
17. W. H. Childs, private communication, 10 June 1986.
18. A. J. Watts, private communication, 12 June 1986.
19. F. Biggs and R. Lighthill, Analytical Approximations for X-ray Cross Sections II, Sandia National Laboratories, Albuquerque, NM, SC-RR-71 0507 (1971).
20. E. F. Plechaty, D. E. Cullen, and R. J. Howerton, Tables and Graphs of Photon-Interactions Cross Sections from 0.1 keV to 100 MeV Derived from the LLL Evaluated-Nuclear-Data Library, Lawrence Livermore National Laboratory, Livermore, CA, UCRL-50400, Vol 6, Rev. 3 (1981).